

RSC Advances



This is an *Accepted Manuscript*, which has been through the Royal Society of Chemistry peer review process and has been accepted for publication.

Accepted Manuscripts are published online shortly after acceptance, before technical editing, formatting and proof reading. Using this free service, authors can make their results available to the community, in citable form, before we publish the edited article. This *Accepted Manuscript* will be replaced by the edited, formatted and paginated article as soon as this is available.

You can find more information about *Accepted Manuscripts* in the [Information for Authors](#).

Please note that technical editing may introduce minor changes to the text and/or graphics, which may alter content. The journal's standard [Terms & Conditions](#) and the [Ethical guidelines](#) still apply. In no event shall the Royal Society of Chemistry be held responsible for any errors or omissions in this *Accepted Manuscript* or any consequences arising from the use of any information it contains.

Theoretical investigation of the chemoselectivity and synchronously pyrazole ring formation mechanism from ethoxymethylenemalononitrile and hydrazine hydrate in the gas and solvent phases: DFT, meta-GGA studies and NBO analysis

H. Sabet-Sarvestani, H. Eshghi, M. Bakavoli, M. Izadyar* and M. Rahimizadeh

Abstract: In this work, structural and kinetic aspects of pyrazole (P) ring formation by reaction of ethoxymethylenemalononitrile (R1) and hydrazine hydrate (R2) have been studied in the gas and solvent phases, theoretically. Two major possible mechanisms have been considered. One of them has been initiated by nucleophilic attack of nitrogen atom of R2 to carbon atom of C=C double bond of R1 (Route 1) and the other has been started by nucleophilic attack of nitrogen atom of R2 to carbon atom of cyanide group in R1 (Route 2). In order to investigate the solvent effect on the reaction mechanism, all possible paths were reconsidered in methanol as the solvent. Obtained results show that the most probable path is route 2 in the gas and solvent phases. Theoretical studies show that chemoselectivity of nucleophilic attack of nitrogen atom in the gas phase is similar to the solvent. Solvent is able to decrease the barrier energy of the rate determining step and enforce the reaction to be proceeded through subroute 5 of route 2.

Keywords: Pyrazole ring; DFT; GGA; Chemoselectivity; NBO analysis; Nucleophilic attack

1. Introduction

Pyrazoles belong to the most important heterocycles containing nitrogen. They are classified as alkaloids, although they are rare in nature. The first natural pyrazole, 1-pyrazolyl-alanine, was isolated from seeds of watermelons.¹ Pyrazole derivatives have attracted considerable interest because of their long history of applications in pharmaceuticals and agrochemicals.² A systematic investigation of this class of heterocyclic lead revealed that pyrazole containing pharmacoactive agents play an important role in medicinal chemistry. The prevalence of pyrazole cores in biologically active molecules has stimulated the need for elegant and efficient ways to make these heterocyclic lead.³ Because of their widespread biological activities, synthesis of pyrazole derivatives is the subject of many research studies. These compounds are reported to possess significant antitumor,⁴ antimicrobial,⁵ anti-inflammatory,⁶ antiviral,⁷ and anticonvulsant⁸ activities.⁹⁻¹⁰

Numerous precursors have been used for the synthesis of pyrazole derivatives. For example, the reaction of β -alkoxyvinyl trichloromethyl ketones with hydrazine hydrochloride leads to ethyl pyrazolecarboxylates.¹¹ The reaction of diethyl ethoxymethylenemalonate with various hydrazine derivatives afforded the 5-hydroxypyrazole-4-carboxylates.¹² In addition the reaction of dimethyl dithiomalonate with methyl hydrazine gave 1-methylpyrazole.¹³ However, syntheses of the pyrazole derivatives have been reported by other precursors such as ethyl ethoxymethylenecyanoacetate,¹⁴ acetylenedicarboxylates¹⁵ and many other compounds.¹⁶⁻¹⁷

Ethoxymethylenemalononitrile is another precursor, which gives 5-aminopyrazole-4-carbonitrile in the presence of hydrazine hydrate.¹⁸ The objective of this study is to provide a theoretical prediction of the kinetic and activation parameters for this reaction. It is also important to elucidate the molecular mechanism associated with this reaction in order to find out a precise idea of the reaction pathway. Experimentally, the reaction has been done in methanol as solvent. For better analysis of the solvent effect, our theoretical studies have been done in solvent and gas phases.

2. Computational details

The structures corresponding to the reactants, transition states and the products for the reaction of pyrazole formation were optimized, using the Gaussian 03 computational package¹⁹ with DFT method as implemented in the computational package. Optimized geometries of the stationary points on the potential energy diagrams were performed using Becke's three-parameter hybrid exchanges functional with the correlation functional of Lee, Yang and Parr (B3LYP) level of theory. The 6-311++G (d,p) basis set which includes a set of d and p-type polarization functions on non-hydrogen and hydrogen atoms, respectively, was used in these calculations. Single point energy calculations on the optimized structures have been done using the meta-GGA functional of MPWB95.²⁰⁻²⁵

2

The synchronous transit-guided quasi-Newton (STQN) method as implemented by Schlegel et al.²⁶ was used to locate the TSs. The intrinsic reaction coordinate (IRC) method²⁷ was also applied in order to check and obtain the profiles connecting the TSs to the two associated minima of the proposed mechanisms.

Vibrational frequencies of the points along the reaction paths were determined to provide an estimation of the zero point vibrational energies (ZPVEs). These calculations verified the nature of the stationary points as minima with real frequencies and the TSs with only one imaginary frequency. Enthalpy, entropy and Gibbs free energy of the reactions were evaluated from the B3LYP data at 298.15K.

Natural bond orbital (NBO) analysis, as suggested by Reed et al.^{28,29} was applied to determine the charge changes in the reaction of pyrazole formation.

Since the solvent-solute interactions are more considerable in the solution, the conductor like polarizable continuum model (CPCM), was applied for calculation of Gibbs free energy of solvation.³⁰

3. Results and discussions

Figure 1 shows the overall reaction. The final product (**P**) is obtained after two nucleophilic attacks of nitrogen atoms of **R2** (Hydrazine) to **R1** (Ethoxymethylenemalononitrile) and elimination of ethanol molecule.

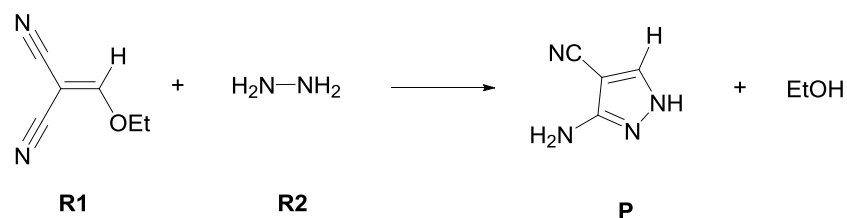


Figure 1. Overall reaction of pyrazole ring formation.

There are eight tautomer isomers for the final product. The corresponding structures for these isomers and calculated total energies in the gas and solvent phases have been reported in table 1. According to their relative energy, tautomer isomer **8** is the preferred structure for the final product.

Table 1. Probable tautomer isomers and their relative Gibbs free energies in the gas phase.

tautomer isomers								
	1	2	3	4	5	6	7	8
Gas phase $\Delta G(\text{kcal.mol}^{-1})$	-0.9	-4.4	-12.8	-14.8	-16.6	-18.5	-37.2	-39.6
Solvent phase $\Delta G(\text{kcal.mol}^{-1})$	10.9	3.8	-6.9	-11.4	-7.8	-8.9	-31.3	-33.0

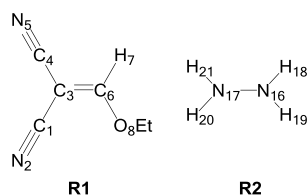


Figure 2. Atom numbering for reactants 1 and 2.

In this research, nucleophilic attack of nitrogen atom and hydrogen transfer has been considered, simultaneously. Two possible mechanisms can be proposed for the synthesis of pyrazole (**P**). Figure 3 shows the first mechanism. It has been initiated by nucleophilic attack of nitrogen atom 17 of **R2** to carbon atom 6 of **R1**. N₁₇-H₂₀ bond has been cleaved while C₃-H₂₀ bond has been formed, simultaneously (for atom numbering see figure 2). Figure 3 shows the most probable intermediates for route 1.

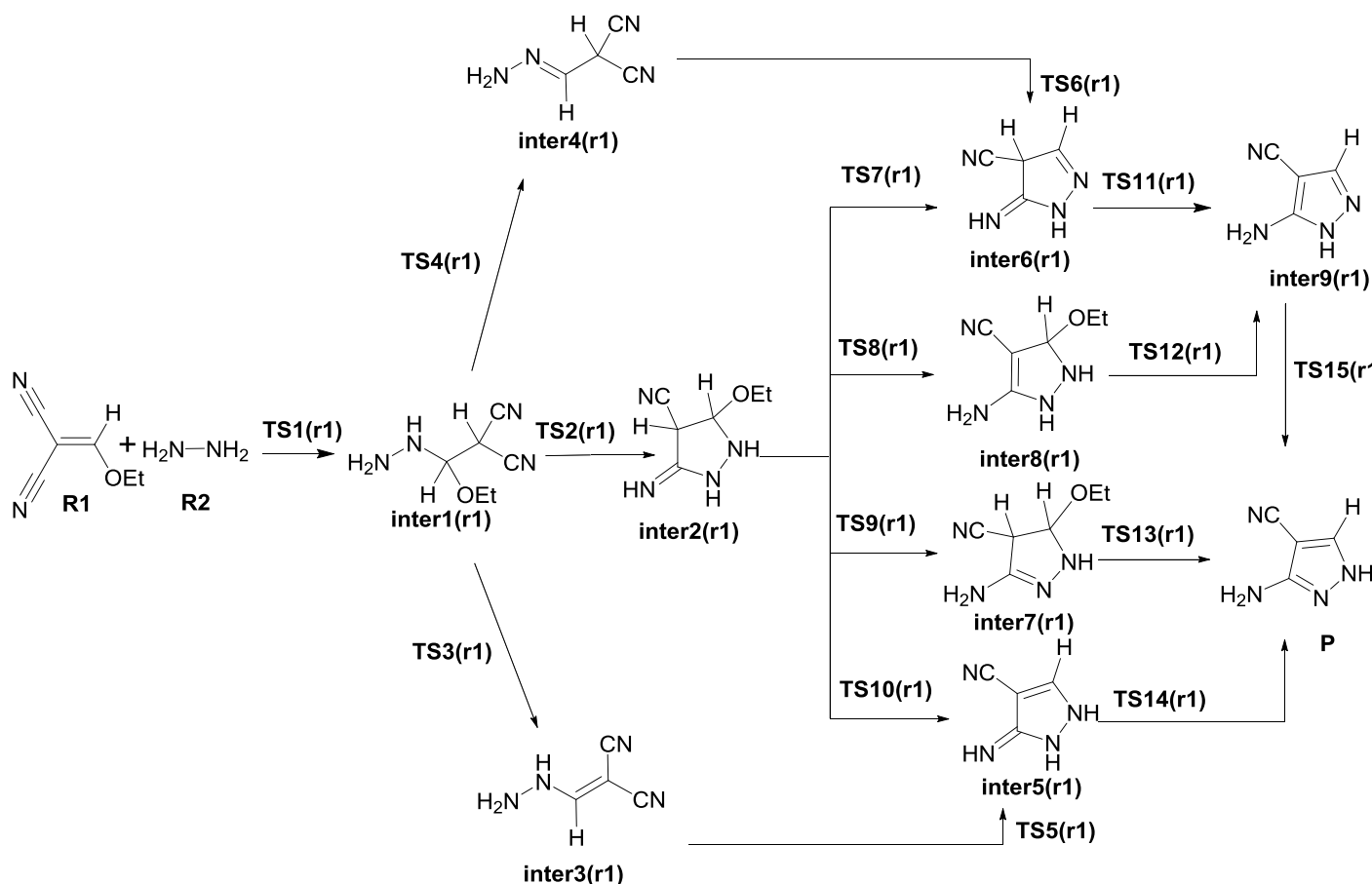


Figure 3. Possible intermediates for route 1.

In the second mechanism, cyanide group of **R1** has been involved in the reaction. The reaction is initiated by nucleophilic attack of nitrogen atom 17 to carbon atom 4; N₁₇-H₂₀ bond has been broken and N₅-H₂₀ bond has been evolved, simultaneously. Figure 4 shows all possible intermediates for route 2.

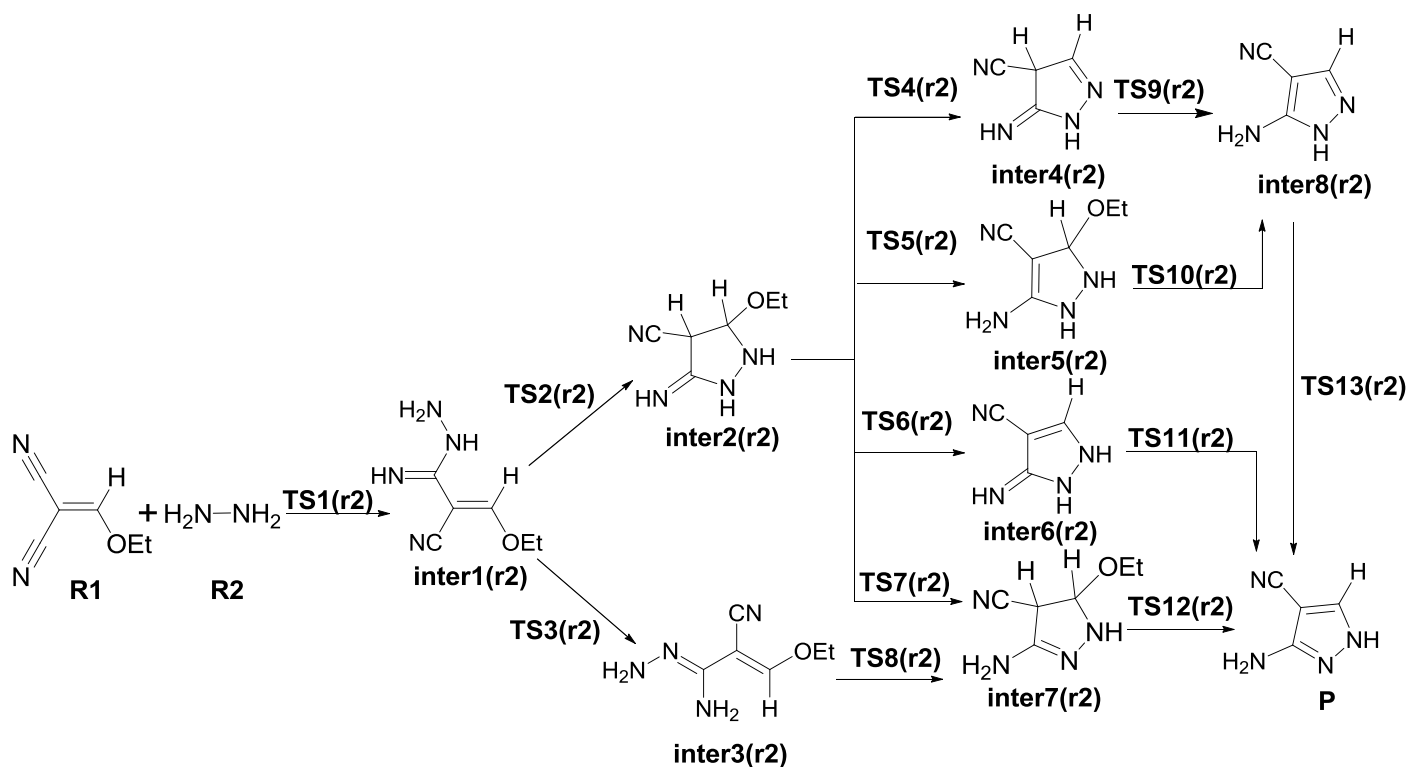


Figure 4. Possible intermediates and TSs for route 2.

Intermediates **7** and **2** are common in two proposed routes and they have two chiral centers. Therefore, different stereoisomers and different energy levels are recognizable. Table 2 shows these diastereomers and their relative energies in the gas phase. Calculated ΔG values for the most stable stereoisomers of the intermediates **2** and **7** are -4.2 and -12.0 kcal.mol⁻¹, respectively. Therefore, the most stable configuration of the stereoisomers have been considered in the overall pathway of the reaction.

Table 2. Diastereomers and relative energy levels of intermediates **7** and **2**.

Diastereomers of intermediate 2		
Absolute Configuration	(3R,4R) and (3S,4S)	(3S,4R) and (3R,4S)
ΔG (kcal.mol ⁻¹)	-2.7	-4.2
Diastereomers of intermediate 7		
Absolute Configuration	(3R,4R) and (3S,4S)	(3S,4R) and (3R,4S)
ΔG (kcal.mol ⁻¹)	-10.6	-12.0

Route 1(r1)

There are three possibilities for the reaction progress through the route 1, after **inter1 (r1)** formation. The first probability leads to **inter2 (r1)** formation, nitrogen atom 16 get involved nucleophilic attack to carbon atom 4, N₁₆-H₁₉ bond has been cleaved and N₅-H₁₉ bond has been formed, simultaneously. The second probability is the elimination of ethanol molecule, yielding **inter3 (r1)**. During this process, C₃-H₂₀ and C₆-O₈Et bonds have been cleaved, EtO₈-H₂₀ bond has been formed and single C₃-C₆ bond has been converted to double bond, simultaneously. Third probability is the elimination of ethanol molecule, yielding **inter4 (r1)**. Instead of C₃-H₂₀ bond breakage, N₁₇-H₂₁ and C₆-O₈Et bonds have been broken, EtO₈-H₂₁ bond has been formed and C₆-N₁₇ bond order has been increased. The corresponding subroutes which includes **inter3 (r1)** and **inter4 (r1)** are known as subroute 3 (blue lines in the potential energy diagrams) and subroute 2 (red lines in the potential energy diagrams), respectively. Also, four subroutes which have been formed from **inter2 (r1)** are known as subroute 1 (black lines), 4 (violet lines), 5 (orange lines) and 6 (green lines).

Route1 is followed through the subroutes 2 and 3. In this process, due to the nucleophilic attack of nitrogen atom 16 of **inter3 (r1)** to carbon atom 4 within N₁₆-H₁₉ bond breaking and N₅-H₁₉ bond formation, **inter5 (r1)** is formed. **inter4 (r1)** has been turned in to **inter6 (r1)** by the same way. The aromatic product has been formed through [1, 3] hydrogen shift of **inter5 (r1)**. During this process, N₁₆-H₁₈ bond is cleaved while N₅-H₁₈ bond is formed. **inter9 (r1)** has been formed through another [1,3] hydrogen shift of **inter6 (r1)**. During this process C₃-H₂₀ bond is cleaved, while N₅-H₂₀ bond is formed and one aromatic intermediate is obtained. Since the relative Gibbs free energy of **inter9 (r1)** is higher than the final product (**P**), [1,5] hydrogen shift is happen. Therefore N₁₆-H₁₈ bond is broken and N₁₇-H₁₈ is formed.

On the other hand, Route 1 can be continued through the **inter2 (r1)**. Two overall processes have been considered for the final product (**P**) formation from **inter2 (r1)**. One of them is ethanol molecule elimination and the other is hydrogen shift. If ethanol elimination is considered as the first process, **inter6 (r1)** and **inter5 (r1)** will be produced from **inter2 (r1)**. **inter5 (r1)** is formed by C₆-O₈Et and C₃-H₂₀ bonds cleavage, while EtO₈-H₂₀ bond is formed and C₃-C₆ single bond order is increased. Then the final product (**P**) has been formed from **inter5 (r1)** by [1,3]-hydrogen shift of H₁₈ from N₁₆ to N₅. As the same way, **inter6 (r1)** is formed from C₆-O₈Et and N₁₇-H₂₁ bonds breaking, while EtO₈-H₂₁ bond is formed and N₁₇-C₆ single bond order is increased. Final product (**P**) is obtained by two hydrogen shifts from the **inter6 (r1)**. One of them is [1,3]-hydrogen shift of H₂₀ from C₃ to N₅ atoms, yeilding **inter9 (r1)** and the other is [1,5]-hydrogen shift of H₁₈ from N₁₆ to N₁₇ atoms. However if the hydrogen shift is considered as the first step, **inter7 (r1)** and **inter8 (r1)** will be formed from the **inter2 (r1)**. **inter7 (r1)** is formed from [1,3]-hydrogen shift of H₁₈ atom from N₁₆ to N₅ atoms, followed by ethanol elimination from **inter7 (r1)**. **inter8 (r1)** and **inter9 (r1)** are obtained by [1,3]-hydrogen shift of H₂₀ atom from C₃ to N₅ and ethanol elimination from **inter8 (r1)**, respectively. Finally, the final product (**P**) has been obtained from [1,5]-hydrogen shift of H₁₈ atom from N₁₆ to N₁₇.

Route2 (r2)

After nucleophilic attack of nitrogen atom 17 to carbon atom 4 and **inter1 (r2)** formation, two Probabilities have been considered for this route. **inter2 (r2)** is formed after nucleophilic attack of N₁₆ to C₆, N₁₆-H₁₉ bond has been broken, double C₆-C₃ bond has been converted to single bond and C₃-H₁₉ bond has been formed. Continuation of the route 2 from the **inter1 (r2)** is the same as route 1. On the other hand, **inter3 (r2)** is formed by [1,3] hydrogen shift from N₁₇ to N₅. Through this process N₁₇-H₂₁ bond has been broken, N₅-H₂₁ bond has been formed and single N₁₇-C₄ bond order has been increased. After this stage, **inter7 (r2)** is formed by nucleophilic attack of N₁₆ to C₆ and H₁₉ transfer to C₃ atom. N₁₆-H₁₉ bond has been cleaved, C₃-H₁₉ bond has been formed and double C₃-C₆ bond order has been decreased. Finally, C₃-H₁₉ and C₆-O₈Et bonds have been broken and EtO₈-H₁₉ bond has been formed and the final product has been produced by ethanol elimination. It is worth noting that both routes share some common intermediates. **inter2 (r1)**, **inter5 (r1)**, **inter6 (r1)**, **inter7 (r1)**, **inter8 (r1)** and **inter9 (r1)** is equal to **inter2 (r2)**, **inter6 (r2)**, **inter4 (r2)**, **inter7 (r2)**, **inter5 (r2)** and **inter8 (r2)**, respectively. Table 3 shows ΔG^\ddagger for the rate determining steps (Rds) of all subroutes.

Gas phase studies

Table 1(S) and Table 2(S) show the ZPVE-corrected total energies and relative Gibbs free energy of intermediates, product, and imaginary frequencies for the TSs for two routes in the gas phase, respectively. Cartesian coordinates of the structures have been included in the Supplementary data section. Figures 5 and 6 show the potential energy diagram depicted according to the relative Gibbs free energy of the species involved in two routes. Table 3 shows ΔG^\ddagger for the rate determining steps of all subroutes.

Table 3. Gibbs free energy of activation for the rate determining steps (Rds) in all of subroutes in the gas phase at the B3LYP level.

Gas phase					
Route 1			Route 2		
Subroutes	Steps of subroute	ΔG^\ddagger of Rds(kcal.mol ⁻¹)	Subroutes	Steps of subroutes	ΔG^\ddagger of Rds(kcal.mol ⁻¹)
1(Black lines)	R, TS1(r1), inter1(r1), TS2(r1), inter2(r1), TS8(r1), inter8(r1), TS12(r1), inter9(r1), TS15(r1), P	59.0	1(Blue lines)	R, TS1 (r2), inter1 (r2), TS3 (r2), inter3 (r2), TS8(r2), inter7 (r2), TS12(r2), P	55.0
2(Red lines)	R, TS1(r1), inter1(r1), TS4(r1), inter4(r1), TS6(r1), inter6 (r1), TS11(r1), Inter9 (r1), TS15(r1), P	66.1	2(Red lines)	R, TS1(r2), inter1(r2), TS2(r2), inter2(r2), TS5(r2), inter5(r2), TS10(r2), inter8 (r2), TS13(r2), P	59.4
3(Blue lines)	R, TS1(r1), inter1(r1), TS3(r1), inter3(r1), TS5(r1), inter5(r1), TS14(r1), P	72.6	3(Green lines)	R, TS1(r2), inter1(r2), TS2(r2), inter2(r2), TS4(r2), inter4 (r2), TS9(r2), inter8(r2), TS13(r2), P	59.4
4(Violet lines)	R, TS1(r1), inter1(r1), TS2(r1), inter2(r1), TS7(r1), inter6(r1), TS11(r1), inter9 (r1), TS15(r1), P	58.4	4(Violet lines)	R, TS1(r2), inter1(r2), TS2(r2), inter2(r2), TS6(r2), inter6(r2), TS11(r2), P	59.4
5(Orange lines)	R, TS1(r1), inter1(r1), TS2(r1), inter2(r1), TS9(r1), inter7(r1), TS13(r1), P	58.4	5(Orange lines)	R, TS1(r2), inter1(r2), TS2(r2), inter2(r2), TS7(r2), inter7(r2), TS12(r2), P	59.4
6(Green lines)	R, TS1(r1), inter1(r1), TS2(r1), inter2(r1), TS10(r1), inter5(r1), TS14(r1), P	58.4	—	—	—

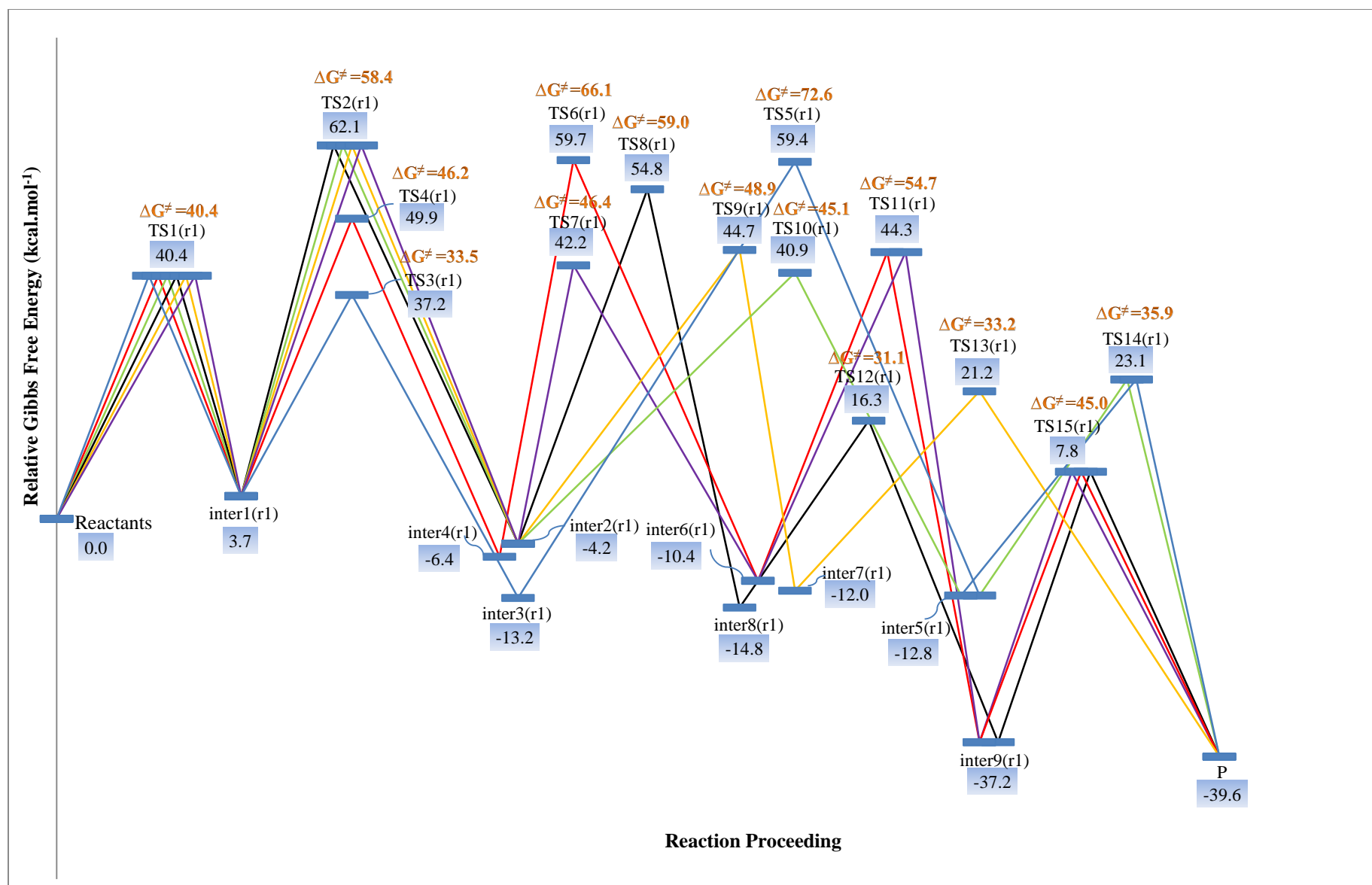


Figure 5. Potential energy diagram, according to the relative Gibbs free energy of the species involved in route1 in the gas phase.

8

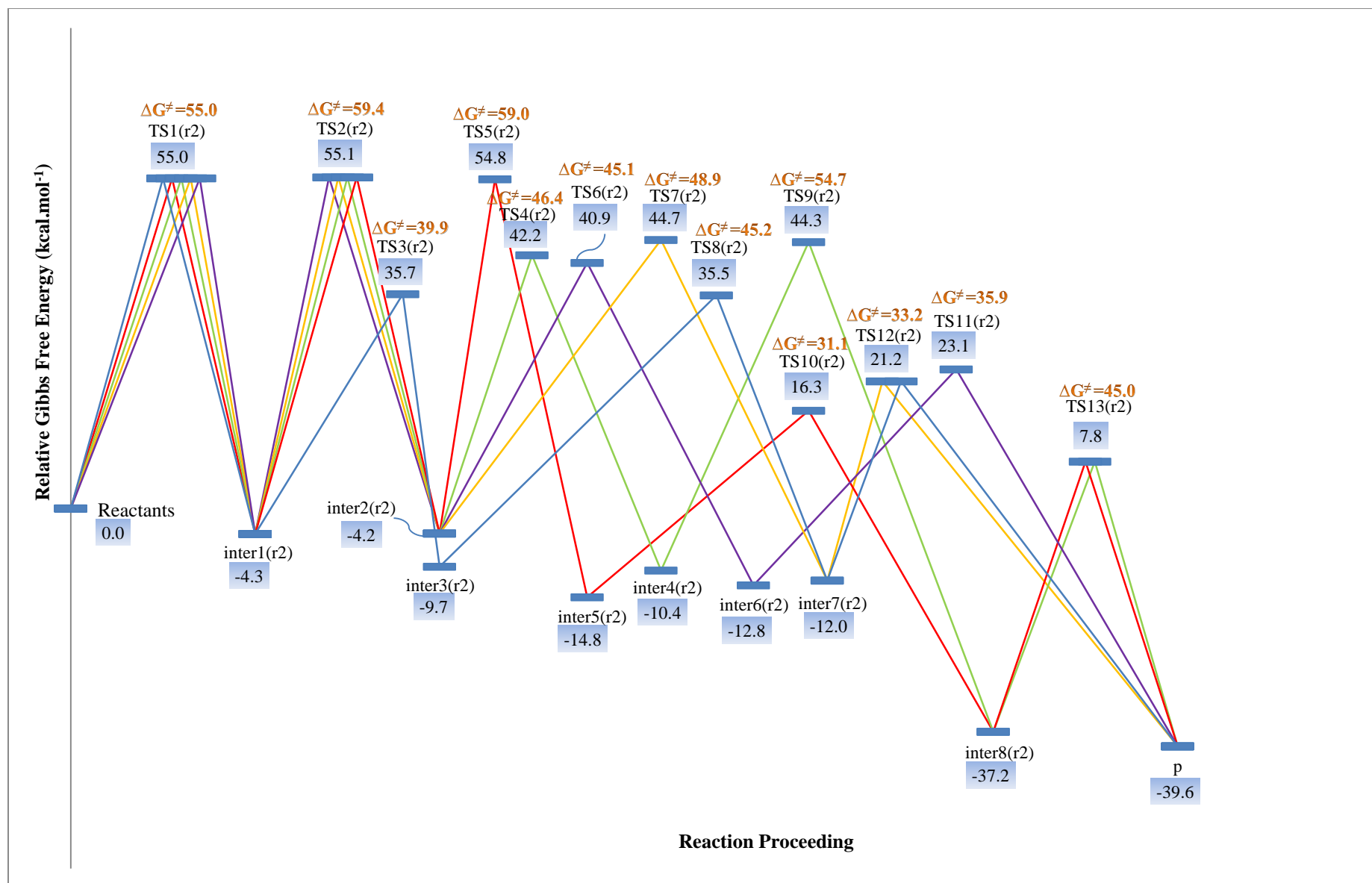


Figure 6. Potential energy diagram, according to the relative Gibbs free energy of the species involved in route 2 in the gas phase.

Simon and Goodman reported geometry optimization and frequency calculation by hybrid GGA functionals, (e.g. B3LYP), followed by a single-point calculation using a hybrid meta-GGA functional, gives reasonably good results compared with transition states optimized with the more expensive hybrid meta-GGA functionals.³¹ Therefore, to develop more accurate and validity of the obtained results for final reaction paths analysis, single point energy calculations on the optimized structures have been done by meta-GGA functional at the MPWB95/6-311++G(d,p) level. Tables 5(S) and 6(S) show the total and relative energies of the intermediates, product and TSs for two routes. Table 4 shows ΔE^\ddagger of rate determining steps in all of subroutes by this method in the gas phase.

Table 4. ΔE^\ddagger for the rate determining steps of all the subroutes in the gas phase at the MPWB95 level.

Gas phase					
Route1			Route2		
Subroutes	Steps of subroute	ΔE^\ddagger of Rds(kcal.mol ⁻¹)	Subroutes	Steps of subroutes	ΔE^\ddagger of Rds(kcal.mol ⁻¹)
1(Black lines)	R, TS1(r1), inter1(r1), TS2(r1),inter2(r1),TS8(r1), inter8 (r1),TS12(r1), inter9 (r1),TS15(r1),P	62.0	1(Blue line)	R, TS1(r2), inter1(r2), TS3(r2), inter3(r2), TS8(r2), inter7 (r2), TS12(r2), P	49.0
2(Red lines)	R, TS1(r1), inter1(r1),TS4(r1),inter4(r1),TS6(r1), inter6(r1),TS11(r1), inter9(r1),TS15(r1),P	62.6	2(Red lines)	R, TS1(r2), inter1(r2),TS2(r2), inter2(r2), TS5(r2), inter5(r2), TS10(r2), inter8 (r2), TS13(r2), P	62.0
3(Blue lines)	R, TS1(r1), inter1(r1),TS3(r1),inter3(r1),TS5(r1),inter5(r1), TS14(r1),P	65.5	3(Green lines)	R, TS1(r2), inter1(r2),TS2(r2), inter2(r2), TS4(r2), inter4 (r2), TS9(r2), inter8 (r2), TS13(r2), P	60.6
4(Violet lines)	R, TS1(r1), inter1(r1), TS2(r1),inter2(r1),TS7(r1), inter6(r1),TS11(r1),inter9 (r1),TS15(r1),P	60.6	4(Violet lines)	R, TS1(r2), inter1(r2),TS2(r2), inter2(r2), TS6(r2), inter6 (r2), TS11(r2), P	79.0
5(Orange lines)	R, TS1(r1), inter1(r1), TS2(r1),inter2(r1),TS9(r1), inter7(r1),TS13(r1),P	57.1	5(Orange lines)	R, TS1(r2), inter1(r2),TS2(r2), inter2(r2), TS7(r2), inter7(r2), TS12(r2), P	54.2
6(Green lines)	R, TS1(r1), inter1(r1), TS2(r1), inter2(r1), TS10(r1), inter5(r1), TS14(r1), P	79.0	—	—	—

At the B3LYP level, subroutes 2 and 3 of the route 1 have larger ΔG^\ddagger for the rate determining step than the other subroutes and other subroutes of two routes have nearly equal ΔG^\ddagger of Rds, exceptionally subroute 1 of route 2,. On the other hand, at the MPWB95 level, ΔE^\ddagger of Rds for subroute 1 is lower than the other subroutes of two routes, significantly. Therefore, both levels of calculations have similar results and it is confirmed that subroute 1 of route 2 (blue line in the potential energy diagrams) is the probable pathway for overall reaction in the gas phase. Since methanol is applied as solvent, investigation of the solvent effects on all of the intermediates and TSs is important.

Solvent phase studies

Experimentally, the reaction has been done in methanol as the solvent. Therefore the solvent effects have been investigated during all of intermediates and TSs on the potential energy diagram. Table 3(S) and Table 4(S) show the ZPVE-corrected total energies and relative Gibbs free energies of the intermediates, product and imaginary vibrational frequencies for the TSs in the solvent phase, respectively. Tables 5 and 6 show ΔG^\ddagger and ΔE^\ddagger of the rate determining steps for all subroutes in methanol, respectively. Since it has been reported the use of hybrid GGA functionals in the geometry optimization step and the Gibbs free energy correction terms followed by single-point energy evaluation using meta-GGA functional, offers a good compromise between accuracy and computational cost³¹, single-point energy evaluation using meta-GGA functional is applied for recognition the most probable pathway for overall reaction.

Table 5. Gibbs free energy of activation for the rate determining steps (Rds) of all subroutes in the solvent phase at the B3LYP level.

Solvent phase					
Route1			Route2		
Subroutes	Steps of subroute	ΔG^\ddagger of Rds(kcal.mol ⁻¹)	Subroutes	Steps of subroutes	ΔG^\ddagger of Rds(kcal.mol ⁻¹)
1(Black lines)	R, TS1(r1), inter1(r1), TS2(r1), inter2(r1), TS8(r1), inter8 (r1), TS12(r1), inter9 (r1), TS15(r1), P	56.2	1(Blue lines)	R, TS1(r2), inter1(r2), TS3(r2), inter3(r2), TS8(r2), inter7 (r2), TS12(r2), P	56.4
2(Red lines)	R, TS1(r1), inter1(r1), TS4(r1), inter4 (r1), TS6(r1), inter6 (r1), TS11(r1), inter9 (r1), TS15(r1), P	62.2	2(Red lines)	R, TS1(r2), inter1(r2), TS2(r2), inter2(r2), TS5(r2), inter5(r2), TS10(r2), inter8 (r2), TS13(r2), P	56.4
3(Blue lines)	R, TS1(r1), inter1(r1), TS3(r1), inter3(r1), TS5(r1), inter5(r1), TS14(r1), P	66.7	3(Green lines)	R, TS1(r2), inter1(r2), TS2(r2), inter2(r2), TS4(r2), inter4 (r2), TS9(r2), inter8 (r2), TS13(r2), P	56.4
4(Violet lines)	R, TS1(r1), inter1(r1), TS2(r1), inter2(r1), TS7(r1), inter6 (r1), TS11(r1), inter9 (r1), TS15(r1), P	56.1	4(Violet lines)	R, TS1(r2), inter1(r2), TS2(r2), inter2(r2), TS6(r2), inter6 (r2), TS11(r2), P	56.4
5(Orange lines)	R, TS1(r1), inter1(r1), TS2(r1), inter2(r1), TS9(r1), inter7 (r1), TS13(r1), P	54.9	5(Orange lines)	R, TS1(r2), inter1(r2), TS2(r2), inter2(r2), TS7(r2), inter7 (r2), TS12(r2), P	56.4
6(Green lines)	R, TS1(r1), inter1(r1), TS2(r1), inter2(r1), TS10(r1), inter5(r1), TS14(r1), P	54.9	—	—	—

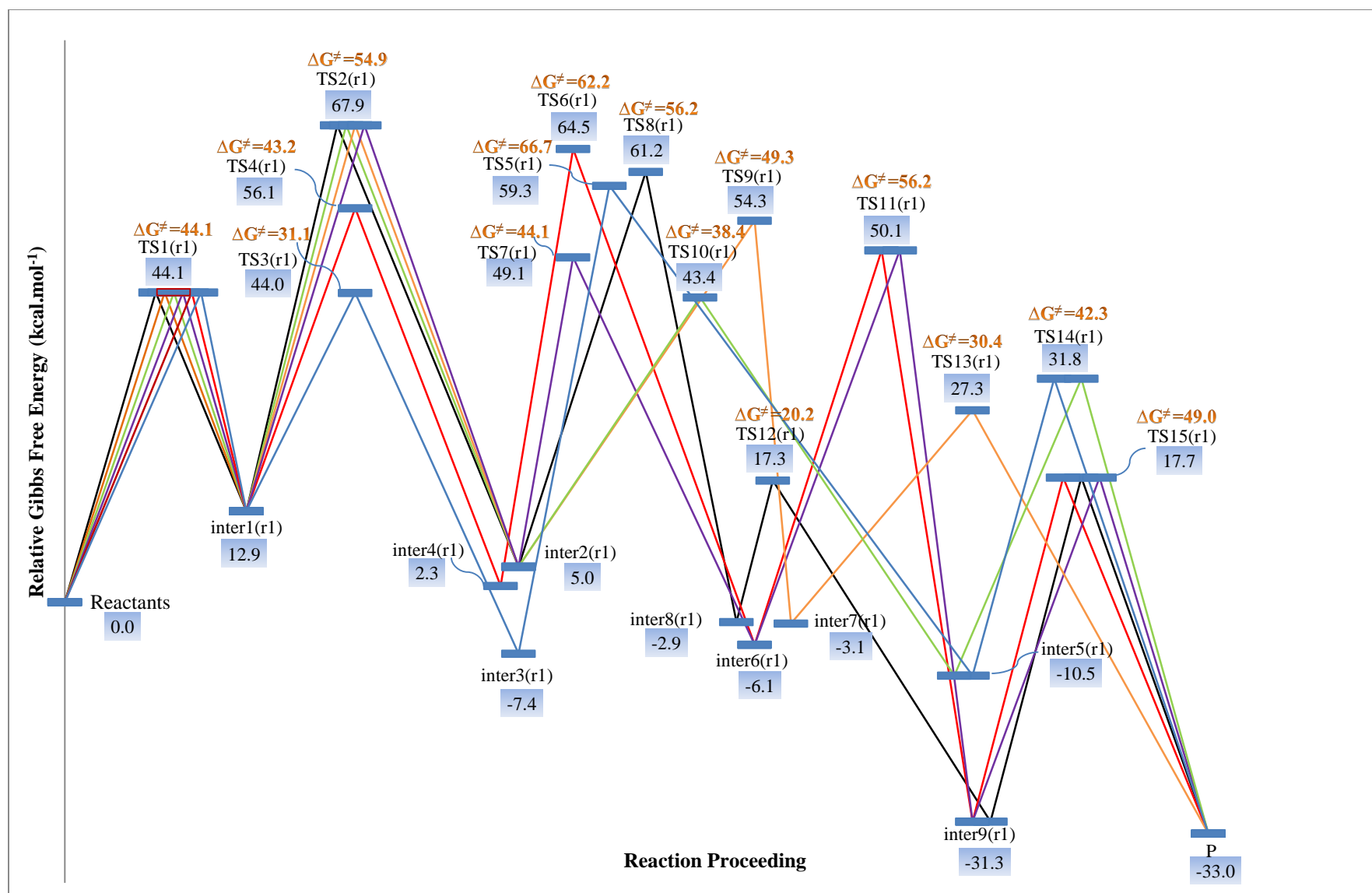


Figure 7. Potential energy diagram, according to the relative Gibbs free energy of the species involved in route1 in the solvent phase.

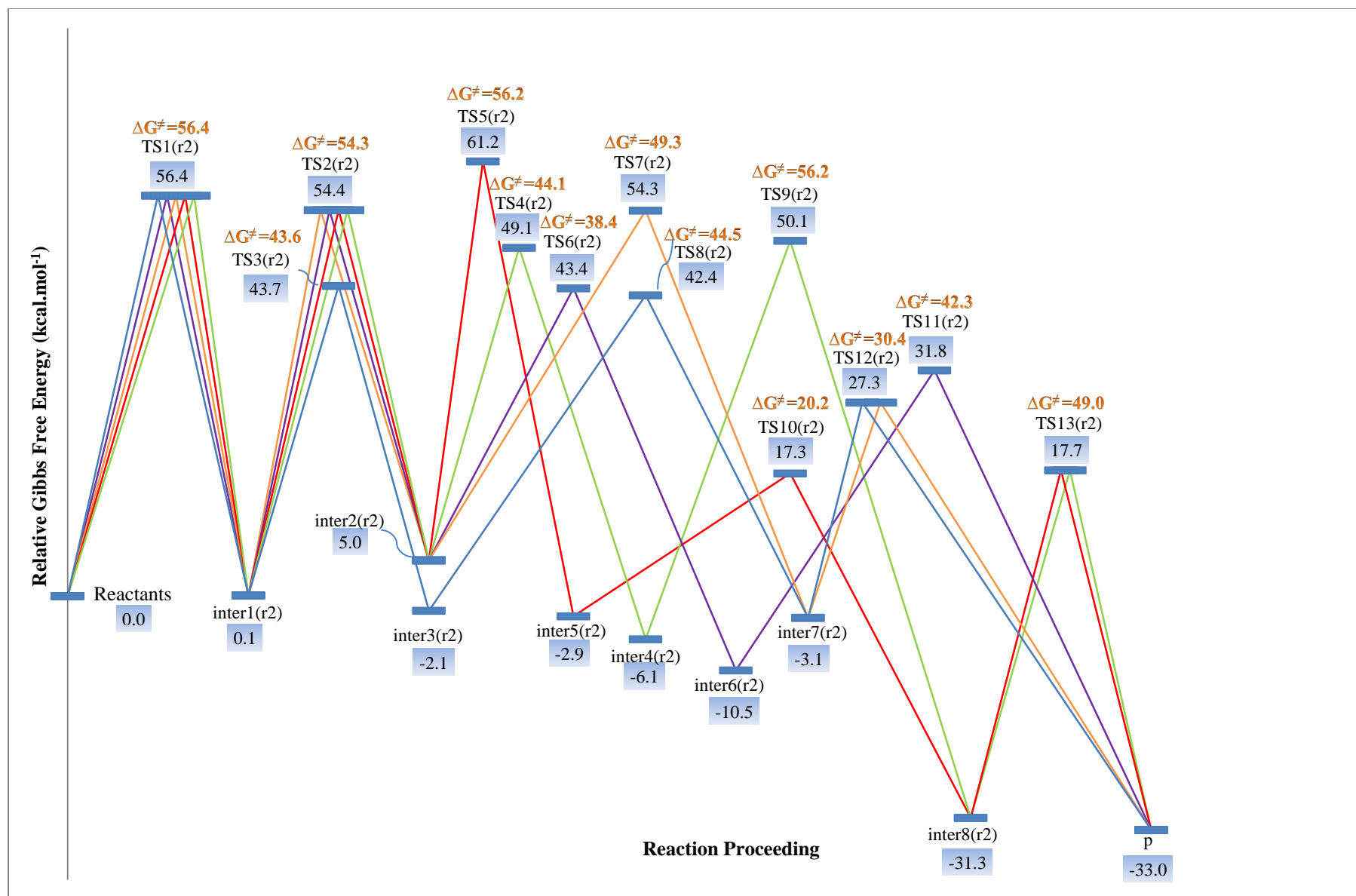


Figure 8. Potential energy diagram, according to the relative Gibbs free energy of the species involved in route 2 in the solvent phase.

Table 7(S) and Table 8(S) show the total energies and relative energies of intermediates, product and TSs for two routes in the solvent phase. Table 6 shows ΔE^\ddagger for the rate determining steps in all of subroutes in the solvent phase. Reaction paths following by the reactants through routes 1 and 2 in the gas and methanol phases have been depicted in Figures 1(S)-4(S).

Table 6. Calculated ΔE^\ddagger for the rate determining steps of all the subroutes in the solvent phase at the MPWB95 level.

Solvent phase					
Route 1			Route 2		
Subroutes	Steps of subroute	ΔE^\ddagger of Rds (kcal.mol ⁻¹)	Subroutes	Steps of subroutes	ΔE^\ddagger of Rds (kcal.mol ⁻¹)
1(Black lines)	R, TS1(r1), inter1(r1), TS2(r1),inter2(r1), TS8(r1),inter8(r1), TS12(r1),inter9(r1), TS15(r1),P	66.0	1(Blue lines)	R, TS1(r2), inter1(r2), TS3(r2), inter3(r2), TS8(r2), inter7 (r2), TS12(r2), P	49.3
2(Red lines)	R, TS1(r1), inter1(r1),TS4(r1), inter4 (r1),TS6(r1), inter6 (r1),TS11(r1), inter9 (r1),TS15(r1),P	61.0	2(Red lines)	R, TS1(r2), inter1(r2),TS2(r2), inter2(r2), TS5(r2), inter5(r2), TS10(r2), inter8 (r2), TS13(r2), P	61.0
3(Blue lines)	R, TS1(r1), inter1(r1),TS3(r1), inter3(r1),TS5(r1), inter5(r1),TS14(r1),P	67.1	3(Green lines)	R, TS1(r2), inter1(r2),TS2(r2), inter2(r2), TS4(r2), inter4 (r2), TS9(r2), inter8 (r2), TS13(r2), P	60.1
4(Violet lines)	R, TS1(r1), inter1(r1), TS2(r1),inter2(r1), TS7(r1),inter6(r1), TS11(r1),inter9(r1), TS15(r1),P	66.0	4(Violet lines)	R, TS1(r2), inter1(r2),TS2(r2), inter2(r2), TS6(r2), inter6 (r2), TS11(r2), P	77.6
5(Orange lines)	R, TS1(r1), inter1(r1), TS2(r1),inter2(r1), TS9(r1),inter7(r1), TS13(r1),P	66.0	5(Orange lines)	R, TS1(r2), inter1(r2),TS2(r2), inter2(r2), TS7(r2), inter7 (r2), TS12(r2), P	44.5
6(Green lines)	R, TS1(r1), inter1(r1), TS2(r1), inter2(r1), TS10(r1), inter5(r1), TS14(r1), P	77.6	—	—	—

At the B3LYP level, all subroutes of two routes have nearly similar ΔG^\ddagger of Rds, exceptionally, subroutes 2 and 3 of the route 1 (high ΔG^\ddagger of Rds). Considering the MPWB95 calculations, it can be seen that subroutes 1 and 5 of the route 2 have low ΔE^\ddagger for the rate determining steps. Therefore, B3LYP and MPWB95 data comparison shows that subroutes 1 and 5 of the route 2 are the probable pathways for the overall reaction. Since subroute 5 has lower ΔE^\ddagger of the Rds, this subroute can be considered as the most probable subroute for the overall reaction.

NBO analysis

Delocalization of electron density between occupied Lewis type (bonds or lone pairs) NBO orbitals and formally unoccupied (anti-bonds and Rydbergs) non Lewis NBO orbitals corresponds to a stabilizing donor–acceptor interaction.³²⁻³³ The energy of these interactions can be estimated by second order perturbation theory. Table 7 shows the energies of donor–acceptor interactions for the **Reactants** and **TS1 (r2)** in the gas and solvent phases. According to this table, the energy difference for the **Reactants** and **TS1 (r2)** in solvent phase is higher than the gas phase. Interactions of lone pair of N5 with $\sigma^*N_{17}-H_{21}$ and $\sigma^*C_3-C_4$ are the most important interaction because it has been increased more than other interactions. Therefore, in the rate determining step of the reaction, solvent molecules have remarkable effect in the barrier energy reduction of **TS1 (r2)**.

Table 7. Electron delocalization energies (E2) in the rate determining step of the reaction in gas and solvent phases at the B3LYP level (kcal.mol⁻¹)

Gas phase				Solvent phase			
Donor	Acceptor	Reactants	Ts1(r2)	Donor	Acceptor	Reactants	Ts1(r2)
πC_3-C_6	$\pi^* C_1-N_2$	21.7	19.1	πC_3-C_6	$\pi^* C_1-N_2$	25.0	23.5
πC_3-C_6	$\pi^* C_4-N_5$	20.5	12.2	πC_3-C_6	$\pi^* C_4-N_5$	23.5	15.6
πC_4-C_5	$\pi^* C_3-N_6$	-	10.9	LP N2	RY*C1	18.1	18.4
LP N2	RY*C1	17.8	17.7	LP N2	$\sigma^* C_1-C_3$	11.0	11.1
LP N2	$\sigma^* C_1-C_3$	11.5	11.8	LP N5	RY*C4	18.5	14.3
LP N5	$\sigma^* C_3-C_4$	11.3	25.9	LP N5	$\sigma^* C_3-C_4$	10.6	24.8
LP N5	RY*C4	18.1	12.7	LP N2	RY*C4	-	12.1
LP N5	$\sigma^* C_4-N_{17}$	-	40.7	LP N5	$\sigma^* C_4-N_{17}$	-	31.2
LP N5	$\sigma^* N_{17}-H_{21}$	-	94.3	LP N5	$\sigma^* N_{17}-H_{21}$	-	103.4
LP O8	$\pi^* C_3-C_6$	45.0	32.4	LP O8	$\pi^* C_3-C_6$	50.5	40.4
$\pi^* C_3-C_6$	$\pi^* C_1-N_2$	11.0	10.4	$\pi^* C_3-C_6$	$\pi^* C_1-N_2$	13.0	14.1
$\pi^* C_3-C_6$	$\pi^* C_4-N_5$	11.2	10.8	$\pi^* C_3-C_6$	$\pi^* C_4-N_5$	13.0	16.8
$\sigma^* C_4-N_{17}$	$\sigma^* N_{16}-N_{17}$	-	10.0	$\sigma^* C_4-N_{17}$	$\sigma^* N_{16}-N_{17}$	-	15.0
Total		168.1	308.9	Total		183.2	340.7
$\Delta E_{\text{delocalization}}$		140.8		$\Delta E_{\text{delocalization}}$		157.5	

Conclusion

A computational study on the kinetics and mechanism of ethoxymethylenemalononitrile (R1) and hydrazine hydrate (R2) reaction has been performed in two media. The reaction can be initiated by nucleophilic attack of nitrogen atom of R2 to carbon atom of C=C double bond of R1 or to cyanide group of R2. CPCM calculations in methanol phase showed that solvent molecules have noticeable effect on the Gibbs free energy of activation and relative Gibbs free energy of species. Nucleophilic attack of nitrogen atom of R1 to carbon atom of cyanide group of R2 is the most probable pathway in the gas and solvent phases. The calculated activation energies are too high for a process which takes place under conventional experimental conditions. It may indicate that solvent molecules or a second substrate molecule is playing an explicit role in the reaction mechanism, but this possibility is beyond the scope of this study.

Acknowledgments

Research Council of Ferdowsi University of Mashhad is acknowledged for financial support of this work.

Notes and references

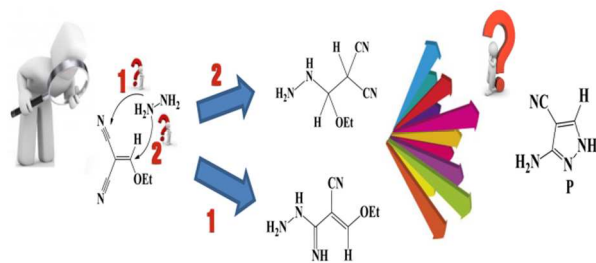
Department of Chemistry, Faculty of Sciences, Ferdowsi University of Mashhad, Mashhad 91775- 1436, Iran.

Corresponding author. Tel/Fax: ++985118795457 e-mail: izadyar@um.ac.ir

1. T. Eicher, S. Hauptmann, *The Chemistry of Heterocycles: Structure, Reactions, Syntheses, and Applications*, 2nd Ed, Wiley-VCH, ISBN 3527307206, 2003.
2. (a) J. Elguero, *Comprehensive Heterocyclic Chemistry*, II(Ed, A. R. Katritzky, C. W. Rees, E. F. V. Scriven), Pergamon, Elsevier Science Ltd., Oxford, 1996, Vol. 3; (b) T. Eicher, S. Hauptmann, A. Speicher, *The Chemistry of Heterocycles*, 2nd Ed, Wiley-VCH, New York, 2003.
3. T. Eicher, S. Hauptmann, *The Chemistry of Heterocycles: Structure, Reactions, Syntheses, and Applications*, Wiley-VCH, 2nd Ed, ISBN 352730720, 2003.
4. L. Peng-Cheng, L. Z. Hai, L. Huan-Qiu, J. Sun, Y. Zhou, *Bioorg. Med. Chem.*, 2010, **18**, 4606.
5. R. Sridhar, P. J. Perumal, S. Etti, G. Shanmugam, M. N. Ponnuswamy, V. R. Prabavathy, N. Mathivanan, *Bioorg. Med. Chem. Lett.*, 2004, **14**, 6035.
6. A. Burguete, E. Pontiki, D. Hadjipavlou-Litina, R. Villar, E. Vicente, B. Solano, S. Ancizu, S. Pe´rezSilanes, I. Aldanaa, A. Monge., *Bioorg. Med. Chem. Lett.*, 2007, **17**, 6439.
7. A. E. Rashad, M. I. Hegab, R. E. Abdel-Megeid, J. A. Micky, F. M. E. Abdel-Megeid, *Bioorg. Med. Chem.*, 2008, **16**, 7102.
8. S. K. Sahu, M. Banerjee, A. Samantray, C. Behera, M. A. Azam, *Tropical J. Pharm. Research.*, 2008, **7**, 961.
9. A. Chauhan, P. K. Sharma, N. Kaushik, *Int. J. Chem. Tech. Res.*, 2011, **3**, 11.
10. A. Jamwal, A. Javed, V. Bhardwaj, *J. Pharm. BioSci.*, 2013, **3**, 114.
11. M. A. P. Martins, R. Freitag, A. F. C. Flores, N. Zanatta, *Synthesis*, 1995, **12**, 1491.
12. W. Holzer, E. Schmid, *J. Het. Chem.*, 1995, **32**, 1341.
13. W. Holzer, H. Gruber, *J. Het. Chem.*, 1995, **32**, 1351.
14. Y. Kurasawa, R. Miyashita, H. S. Kim, Y. Okamoto, *J. Het. Chem.*, 1995, **32**, 671.
15. Y. Kurasawa, A. Takano, K. Kato, A. Takada, H. S. Kim, Y. Okamoto, *J. Het. Chem.*, 1996, **33**, 757.
16. K. Makino, H. S. Kim, Y. Kurasawa, *J. Het. Chem.*, 1998, **35**, 489.
17. K. Makino, H. S. Kim, Y. Kurasawa, *J. Het. Chem.*, 1999, **36**, 321.
18. H. G. Hitchings, E. A. Falco, 1956, US 2,759,949, 1957, CA 11391g.
19. M. J. Frisch, G. W. Trucks, H. B. Schlegel, et al, Gaussian 03, Revision B.03, Gaussian, Inc, Wallingford, CT, US, 2004.
20. A. D. Becke, *Phys. Rev. A.*, 1988, **38**, 3098.
21. C. Lee, W. Yang, R. G. Parr, *Phys. Rev. B.*, 1988, **371**, 785.
22. K. Raghavachari, J. S. Binkley, R. Seeger, J. A. Pople, *J. Chem. Phys.*, 1980, **72**, 650.
23. C. Tratz, P. L. Fast, D. G. Truhlar, *Phys. Chem. Commun.*, 1999, **2**, 9.
24. A. D. McLean, G. S. Chandler, *J. Chem. Phys.*, 1980, **72**, 5639.
25. E. A. Salter, G. W. Trucks, R. J. Bartlett, *J. Chem. Phys.*, 1989, **90**, 1752.
26. H. B. Schlegel, C. Peng, P. Y. Ayala, M. J. Frisch, *J. Comput. Chem.*, 1996, **17**, 49.
27. K. Fukui, *J. Phys. Chem.*, 1970, **74**, 4161.
28. A. E. Reed, L. A. Curtiss, F. Weinhold, *Chem. Rev.*, 1988, **88**, 899.
29. A. E. Reed, R. B. Weinstock, F. Weinhold, *J. Chem. Phys.*, 1983, **78**, 4066.
30. M. Cossi, V. Barone, R. Cammi, J. Tomasi, *Chem. Phys. Lett.*, 1996, **255**, 327.
31. L. Simon, J. M. Goodman, *Org. Biomol. Chem.*, 2011, **9**, 689.
32. M. Izadyar, M. Khavani, *International Journal of Quantum Chemistry.*, 2014, **114**, 666.
33. M. Izadyar, M. Gholizadeh, M. Khavani, M. R. Housaindokht, *J. Phys. Chem. A.*, 2013, **117**, 2427.

Supplementary Material

Optimized structures of the TSs have been included in the Supplementary data section. Supplementary data associated with this article can be found, in the online version, at....



Chemoselectivity of nucleophilic attack of nitrogen atom has been changed in the presence of the solvent due to rds changes.